Journal of the Energy Institute 89 (2016) 793–806

Contents lists available at ScienceDirect

Journal of the Energy Institute

journal homepage: http://www.journals.elsevier.com/journal-of-the-energy-institute

An investigation of methane and propane vertical flares

Alechenu A. Aboje, James I. Erete, Kevin J. Hughes, Lin Ma, Mohamed Pourkashanian, Alan Williams*

Energy Technology and Innovation Initiative, University of Leeds, Leeds LS2 9JT, UK

ARTICLE INFO

Article history:
Received 4 February 2015
Received in revised form
13 March 2015
Accepted 16 March 2015
Available online 23 March 2015

Keywords:
Flares
Diffusion flames
Flame length
Flame lift-off height
Pollutant

ABSTRACT

Flame lengths, temperature, species and lift-off heights have been experimentally and numerically investigated and compared for buoyant methane and propane jet diffusion flames at Reynolds number of 5700. The flow field has been modeled using the Reynolds-Averaged Navier–Stokes equation incorporating the k–ε realizable turbulence closure model. Combustion was modeled using the unsteady Eulerian-flamelet model based on the mixture fraction approach and the heat loss by radiation was accounted for using the Discrete Ordinates Method. The GRI mech. 3.0 and the CRECK reaction mechanisms were used to model the kinetics of the methane and propane reactions, respectively. Comparison of the predicted flame length and temperature revealed good agreement with experimental data. Post-flame measurements of NO_x and CO revealed greater quantities of both pollutants in the methane flame. Furthermore, investigation of the effect of the burner nozzle thickness on the flame lift-off heights showed that the lift-off height decreased as the nozzle thickness was increased, with the methane flame displaying higher lift-off heights.

1. Introduction

The combustion of waste hydrocarbons in flares is associated with the undesirable formation of pollutants, such as CO, NO_x, unburned hydrocarbons, smoke as well as CO_2. Many studies have been made of methane and natural gas flames but relatively few have been made of propane flames. Thus many generalizations about flare behavior have been concerned only with methane flames. This investigation is concerned with the difference in behavior between methane and propane flames when compared on the basis of similar Reynolds number. Flame lengths are important in flaring applications because they determine the height of the flare stack and historically a considerable number of studies have been made of flame lengths of methane and propane flames and a number of correlations have been made based on jet properties. Semi-empirical correlations have been derived for the length of a flare flame and the radiation from the flame by representing the flame surface as the frustum of a right cone [1]. It has also been demonstrated that the flame length decreases as the enthalpy of combustion of the fuel is reduced and increases with an increase in the pipe internal diameter for a given fuel at a given flow rate [2,3]. The stability of flares is also of major importance due to the effect it has on combustion efficiency and pollutant emissions. The EPA reported that "properly operated flares achieve at least 98% combustion efficiency in the flare plume". According to the EPA, this relatively high efficiency is achieved by stable flames, with a fuel enthalpies of combustion in the flared gases of at least 7.5–9.3 MJ/m^3. The flame stability has been defined as the condition where a decrease in the flare gas heating value or an increase in flare gas exit velocity results in flame blow-out [4]. For many hydrocarbon fuels, the burner-detached (lifted) flames can only survive at cross-flow velocities lower than 8 m/s [5]. In comparison, the burner attached flames can exist at much higher crosswind velocities than lifted flames. This is important in flares where blowouts are a common problem. Research carried out by the ARC helped to establish the significance of a crosswind on flare efficiencies, a factor which was overlooked in the EPA research, where most of the studies conducted related to natural gas flares.

The advance made in computing technology has enabled researchers to model the properties of turbulent jet diffusion flames using numerical techniques. In-flame temperatures and species as well as soot have been successfully modeled by several authors with good agreements with experimental data [6–8]. A recent study of variants of the k–ε turbulence closure models has shown that the realizable

* Corresponding author.
E-mail address: A.Williams@leeds.ac.uk (A. Williams).

http://dx.doi.org/10.1016/j.joei.2015.03.009
1743-9671/

version is superior to the other variants in modeling diffusion flames from circular pipe burners [9]. The present work is both a numerical and an experimental investigation of turbulent jet diffusion flames of propane and methane operating under similar conditions with an aim to investigate the differences that exist between the flames in terms of their flame lengths, the emission from the flames and the effect that a change in the thickness of the pipe-nozzle will have on the flame lift-off heights.

2. Experimental methods

The experimental work was performed on a laboratory scale diffusion burner with a fuel pipe with internal and external diameters of 3.25 mm and 6.4 mm respectively. The burner featured a shroud with a diameter of 102 mm, through which shroud-air was supplied at about 0.3 m/s which served to shield the flame from surrounding disturbances.

2.1. Flame length and lift-off height measurement

Both the visible flame lengths – defined as the axial distance between the burner exit plane and the tip of the visible flame, and the lift-off heights of the flames – defined as the distance between the nozzle and the base of the lifted flame, were obtained by averaging a video record of the flames over 30 frames using a 12.1 megapixels CMOS camera (Canon PowerShot SX260HS).

2.2. Flame temperature measurement

The burner was mounted on a three-dimensional (XYZ) traverse grid system, and the origin was centered at the exit plane of the burner tube. The fuel flow rate was measured using a calibrated rotameter, and the average jet velocity u_j, was calculated from the fuel flow rate. Radial measurements of the in-flame temperature were taken at 3 axial flame locations using a Pt–Pt/13-%-Rh thermocouple with a bead diameter of 216 μm. The thermocouple was coated with a thin layer of silica to avoid catalytic reactions on the bead [10]. The output of the thermocouple was processed by a computer controlled data acquisition system and the data were later corrected for radiation and convection heat transfer between the thermocouple bead and the surroundings using the method of Kaskan [11].

2.3. Species and soot measurement

Gas samples were extracted at the post flame region using a quartz probe with a 1 mm tip diameter. The samples withdrawn through the probe were then passed through a heated sample line to a Horiba VS-3000 gas conditioning system and passed into a Horiba VA 3000 chemiluminescent NO_x analyzer and an infrared CO/CO_2 analyzer. The total unburnt hydrocarbons in the post-flame region were determined using a MEXA-1170 HFID flame ionization detector (FID). The gas analyzers were calibrated with certified standard mixtures of 52 ppm, 8.02%, and 6.25% of NO, CO and CO_2 in nitrogen, respectively. Zero and span calibrations were performed before and after each measurement in order to minimize the influence of the instrument drift.

The soot mass in the post flame region was determined gravimetrically using filter papers in a holder. The filter papers were dried in an oven and weighed before soot deposition. The fuels were combusted on a basis of similar Reynolds number and the filter paper was re-weighed to determine the mass of soot collected. Several runs were carried out for each fuel, and the average mass was determined.

3. Numerical methods

3.1. Mathematical models

The mathematical models available in the commercial CFD software package ANSYS [12] were used to simulate the experimental conditions. The code solves the density-averaged form of the balance equations for mass, momentum, energy and the relevant scalar quantities describing turbulence and combustion based on the finite volume solution method. The flow field has been modeled using the RANS equation. The Reynolds stresses arising from the RANS equations were closed using the realizable k–ε turbulence model. Combustion was modeled with the laminar flamelet model [13], while the radiation was modeled with the discrete ordinate model [14].

The governing equations used for the analysis of the turbulent reacting flows are given below in Cartesian tensor notation.

Mass conservation:

$$\frac{\partial \overline{\rho}}{\partial t} + \frac{\partial}{\partial x_k}(\overline{\rho}\tilde{u}_k) = 0 \tag{1}$$

Momentum conservation:

$$\frac{\partial(\overline{\rho}\tilde{u}_i)}{\partial t} + \frac{\partial}{\partial x_k}(\overline{\rho}\tilde{u}_k\tilde{u}_i) = \frac{\partial \overline{P}}{\partial x_i} + \frac{\partial \tau_{ik}}{\partial x_k} + \tilde{F}_k - \frac{\partial}{\partial x_k}\left(\widetilde{\rho u_k'' u_i''}\right) \tag{2}$$

where $\overline{\rho}$ and $\overline{P}$ are the unweighted mean density and pressure; the symbol $\sim$ represents a Favre mean or density weighted mean quantity and the symbol $''$ denotes a corresponding fluctuating quantity. The two terms on the left hand side of Equation (2) represent the accumulation and convective terms respectively. The first three terms on the right hand side represent the pressure, viscous and source terms respectively, while the last term represents the turbulence or Reynolds stress.

Energy conservation:

$$\frac{\partial\left(\overline{\rho}\tilde{h}\right)}{\partial t}+\frac{\partial}{\partial x_k}\left(\overline{\rho}\tilde{u}_k\tilde{h}\right)=\frac{\partial}{\partial x_k}\left(\frac{\mu}{Pr}\widetilde{\frac{\partial h}{\partial x_k}}\right)+q_{rad}-\frac{\partial}{\partial x_k}\left(\widetilde{\rho u_k'' h''}\right) \tag{3}$$

where $\tilde{h}$ and h'' are the mean and fluctuating part of the sensible enthalpy, respectively. μ and Pr represent the dynamic viscosity and the Prandtl number, respectively and q_{rad} is the volumetric heat loss due to radiation. The sensible enthalpy is defined as:

$$\tilde{h}=\int_{T_{ref}}^{\tilde{T}} C_{p,mix}\left(\tilde{T}\right)d\tilde{t} \tag{4}$$

where $C_{p,mix}$ is the constant specific heat capacity of the mixture and T_{ref} is a reference temperature.

Species Conservation:

$$\frac{\partial\left(\overline{\rho}\tilde{Y}_i\right)}{\partial t}+\frac{\partial}{\partial x_k}\left(\overline{\rho}\tilde{u}_k\tilde{Y}_i\right)=\frac{\partial}{\partial x_k}\left(\rho D_i\widetilde{\frac{\partial Y_i}{\partial x_k}}\right)+\widetilde{\dot{w}_i}-\frac{\partial}{\partial x_k}\left(\widetilde{\rho u_k'' Y_i''}\right) \tag{5}$$

where $\tilde{Y}_i$ and Y_i'' are the mean and fluctuating mass concentrations of species i, $\overline{\rho}\widetilde{u_k'' Y_i''}$ is the turbulent mass flux and $\widetilde{\dot{w}_i}$ is the source term, representing the mean reaction rates. As obtained in numerous numerical studies of turbulent jet flames, the turbulent momentum fluxes or Reynolds stresses, $\rho\widetilde{u_k'' u_i''}$ are obtained using a turbulence model. Further, the heat and mass fluxes, $\rho\widetilde{u_k'' h''}$ and $\overline{\rho}\widetilde{u_k'' Y_i''}$ are obtained using the gradient transport approach [15] with a constant turbulent Schmidt and Prandtl number.

3.2. Combustion model

The laminar flamelet model is based on the concept of a conserved scalar – the mixture fraction [16]. The mixture fraction is conserved throughout the flow field because its definition is based on conserved quantities. Furthermore, the model assumes unity Lewis number i.e. the diffusivities of species occur at the same rates. If a reactive system is considered to be in a state of chemical equilibrium i.e. the chemical reaction rate is much faster than mixing by molecular diffusion, then the instantaneous values of the temperature, densities and mass fractions of species depended solely on the mixture fraction, Z.

$$\phi_i=\phi_i(Z), \qquad \phi=\rho, T, Y_i \tag{6}$$

where ϕ_i represents the instantaneous density, temperature or mass fraction of species respectively. The presence of turbulence in a flow field introduces fluctuations in the mixture fraction and in the scalar variables, therefore, the relation between the mixture fraction with the reacting species composition and temperature become nonlinear and can no longer be obtained using Equation (6). A PDF approach is therefore used to obtain the mean values of the species composition and temperature by weighing their instantaneous relationship with the mixture fraction. The shape of the PDF can be described by several mathematical functions. However the β-function shape of the PDF (single- and two-mixture-fraction cases) most closely represents the experimentally observed PDFs [17]. The flamelet approach has the advantage over the species transport model, that the flamelet profiles $Y_k=\phi\,(Z,\chi)$ can be pre-computed and stored in a flamelet library dataset with all the required complex chemistry. The library consists of a set of relationships $\phi\,(Z)$ between the scalar flow properties, ϕ and the mixture fraction Z. The variable χ is known as the scalar dissipation rate and it is a function of the mixture fraction gradient which accounts for the turbulence in the flamelets. The PDF integration is performed once prior to the main flow field calculations and based on the PDF integration, the computed instantaneous values of the scalar quantities are stored in a look-up table for subsequent retrieval and updated during the main flow field calculations. This procedure produces significant computational savings compared to solving the transport equations for the individual species.

3.3. Soot and radiation models

Soot formation in the flames was modeled using the Moss and Brookes [18] approach implemented in the Fluent code, in which soot nucleation and growth rates are based on the acetylene concentration as the soot precursor and gas phase specie. Soot oxidation is based on the model by Fenimore and Jones [19] which accounts for soot oxidation by both [O] and [OH] species. Soot formation and soot oxidation are competing processes in a flame and the amount of soot emitted will depend on the balance between these two processes. These processes can be expressed mathematically as:

$$\frac{dM}{dt}=\left(\frac{dM}{dt}\right)_{Inc.}+\left(\frac{dM}{dt}\right)_{Gro.}+\left(\frac{dM}{dt}\right)_{Oxi.} \tag{7}$$

where M represents the soot mass density, the first and second right-hand terms represent rates of soot formation (inception and growth) and the third term represents the rate of soot oxidation. The Discrete Ordinate model was used to account for radiant heat from the flames. The CFD domain was discretized into three angular directions based on the S2 procedure. The effect of soot on radiation was taken into account by including the effect of soot concentration on the radiation absorption coefficient. The soot absorption is calculated using:

$$a_s = b_1 \rho_m [1 + b_T (T - 2000)] \quad (8)$$

where ρ_m is the soot density (kg m^{-3}), and b_T and b_1 are the coefficients obtained from curve fitting to the experimental data [20].

4. Computational details

The computational simulation was achieved on a two-dimensional structured quad mesh generated using the ANSYS-ICEM meshing software. The mesh domain extended 2.3 m (700 d_i) in the axial direction and 0.4 m (123 d_i) in the radial direction (Fig. 1), where d_i is the internal diameter of the pipe. 320 and 77 mesh nodes where used in the axial and radial directions respectively with the origin centered at the burner exit. A mesh refinement study was conducted to ensure the independence of the solution on the mesh size and density. This entailed comparing the velocity and temperature profiles for mesh sizes of 5 E4, 1 E5 and 1.8 E5 cells, respectively (Fig. 2). The mesh distribution option was selected so as to place a finer node distribution in the pipe region and coarser nodes further away from the pipe. Pressure inlet boundary conditions were employed at the entrainment boundaries, located 0.3 0160 m (92 d_i) and 0.4 m (123d_i) away from the burner exit in the axial and radial directions, respectively. A pressure outlet boundary condition was employed at the outflow, located 2 m (615 d_i) away from the burner exit. A no-slip wall boundary condition was implemented at the pipe walls and 5% turbulence intensity was specified at the pipe inlet. The turbulence intensity at the entrainment boundaries were specified at 1% and 0.2% for the pressure inlet and outlet, respectively. Internal emissivity was set to one at all the pressure boundaries. The numerical solution was accomplished using a finite-volume discretization technique implemented in the ANSYS-Fluent solver. All the terms in the flow and combustion equations were discretized using a second-order upwind scheme, and the coupling between the pressure and velocity fields were handled via the SIMPLE algorithm implemented in the Fluent code. All constants in the flow, combustion and soot models were set to the defaults values obtained in the Fluent solver. Residuals for all the solved equations were below 10^{-4} and iteration was continued until a stable residual was obtained. The gas phase combustion was modeled via the laminar flamelet approach and the kinetic of the propane and methane reactions were modeled using the CRECK [21] and GRI [22] reaction mechanisms which contained 113 species with 1901 reactions and 53 species with 325 reactions, respectively. However, only 40 species were utilized in the calculations due to limitations on computing resources.

5. Results and discussion

5.1. Flame lengths

The flame lengths of buoyant methane and propane diffusion flames with Reynolds numbers of about 5700 have been investigated numerically. The pictures of the flames are shown in Fig. 3 and the measured flame lengths are shown in Table 1. The luminosity seen in the propane flame is due to its high soot concentration. The measured visible flame lengths of the methane and propane flames were within the range of 51.6 ± 3.5 cm and 60.7 ± 4.8 cm respectively. The numerical work is an attempt to predict the visible flame length by using the carbon monoxide burn-out height along the flame axis as an indicator of the chemical flame length, as illustrated in Figs. 4 and 5. Carbon monoxide becomes quickly oxidized to carbon dioxide towards the flame tip hence the position along the flame axis where the carbon monoxide concentration falls to zero is a likely indication of where the flame ends. The temperature profile along the flame axis is also investigated as a means for predicting the flame length as shown in Fig. 4(c) and (d). However, the agreement between the predicted result and the experimental data was not as good as that obtained for the carbon monoxide predictions. The predicted flame lengths using the carbon monoxide burn-out position is better appreciated when viewed from the plots in Fig. 5 and it can be observed from the plot that the position along the axis where the carbon monoxide burns out (indicated by the vertical dash on the horizontal axis) approximates the visible flame length quite well. In the case of the propane flame, the prediction shows a better match with the visible flame length, falling within the experimental range of 60 ± 4 cm. However, in the case of methane, there is an under-prediction of the visible flame length by about 6%. Also the methane lift-off height has been under-predicted as shown by the carbon monoxide contour in Fig. 4(a).

5.2. Flame temperature

Predictions of the temperature as a function of axial position for the methane and propane flames are shown in Fig. 6. The plots show that the predicted peak temperature along the flame axis is lower for the propane flame. This is due to the higher concentration of soot in the propane flame which results in increased radiation from the flame, thus lowering the flame temperature. Another reason for the lower flame temperature in propane could be the greater air entrainment along the length of the flame and attached nature of the flame. The predicted peak temperature along the axis for the methane flame is about 2100 K and this is about 6% higher than the experimentally observed peak temperature of 1985 K. The peak axial temperature prediction for the propane flame was about 1800 K, which is 10% higher than the experimentally observed peak temperature of 1700 K. Further downstream of the burner (axial position > 60 cm), the propane flame shows

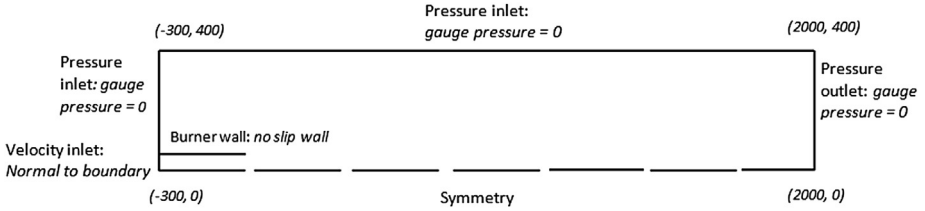

Fig. 1. Computational flow domain showing the boundary conditions.

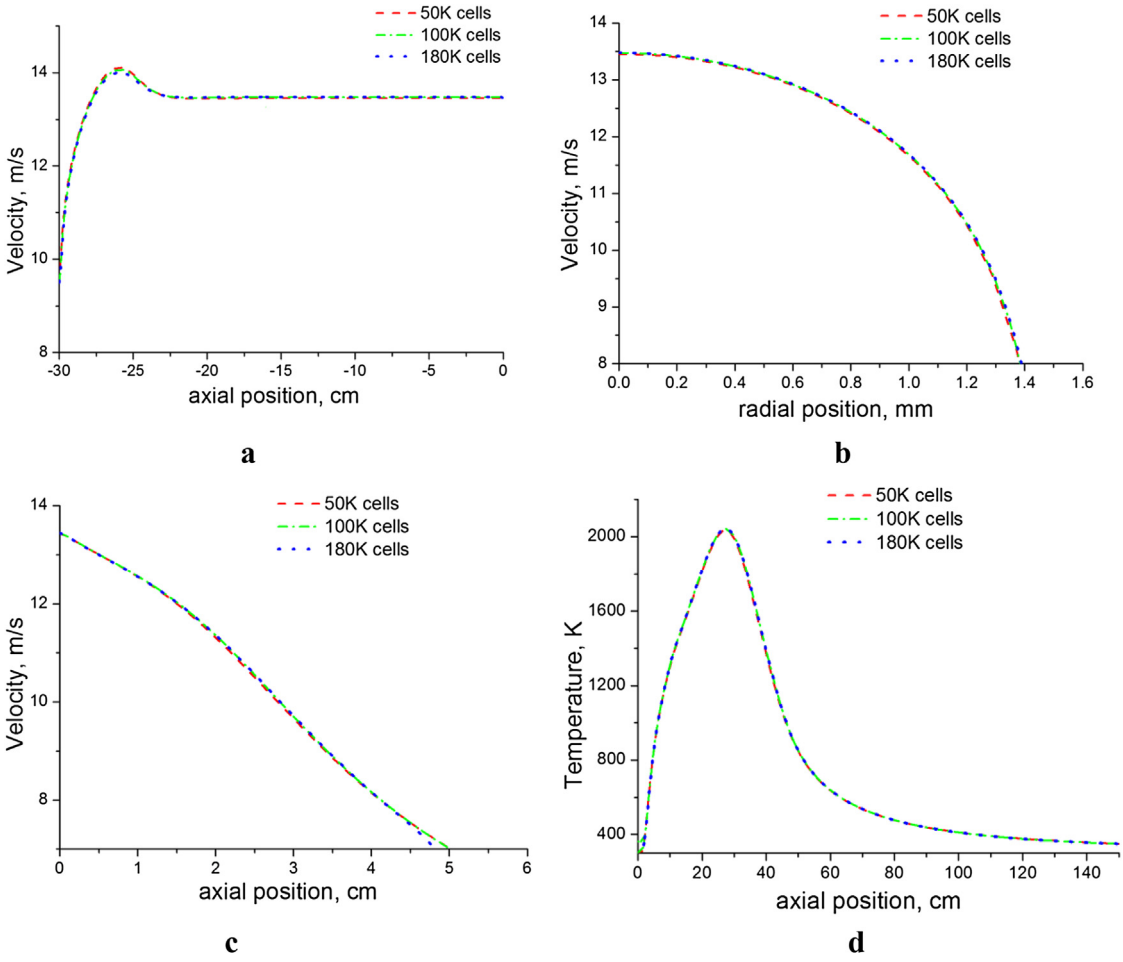

Fig. 2. Predictions of the (a) axial velocity (b) radial velocity (c) velocity at pipe exit and, (d) axial temperature, for 5 E4, 1 E5 and 1.8 E5 mesh sizes for the methane flame.

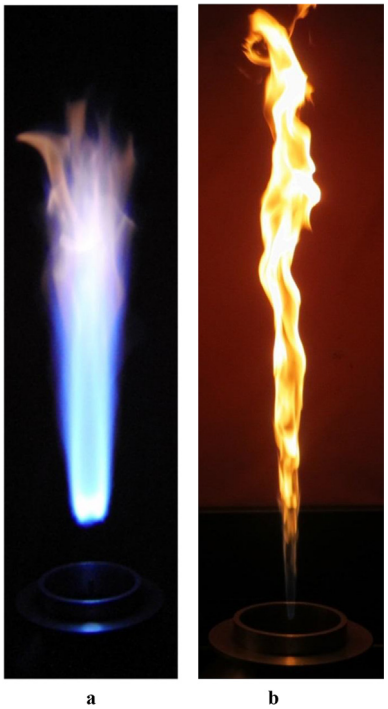

Fig. 3. Photographs of (a) methane flame (b) propane flame at Re = 5700.

Table 1
Flame properties.

Parameter	Methane	Propane
Reynolds number	5700	5700
Froude number	21,000	1800
Jet velocity (m/s)	27	7.6
Shroud velocity (m/s)	0.3	0.3
Visible flame length (cm)	51.6 ± 3.5	60.7 ± 4.8
Lift off height (cm)	8.5 ± 2.7	–

higher temperatures along the axis because it is about 15% longer than the methane flame. Fig. 7 shows the prediction of the temperature as a function of radial position for the methane (a–c) and propane (d–f) flames. The predictions are compared with experimental data, and from the comparison we observe that the temperature predictions are better upstream of the flame, towards the burner nozzle for both flames. Downstream of the flame and towards the flame-tip region (x/d = 94), the predictions deteriorate due to increased flame turbulence.

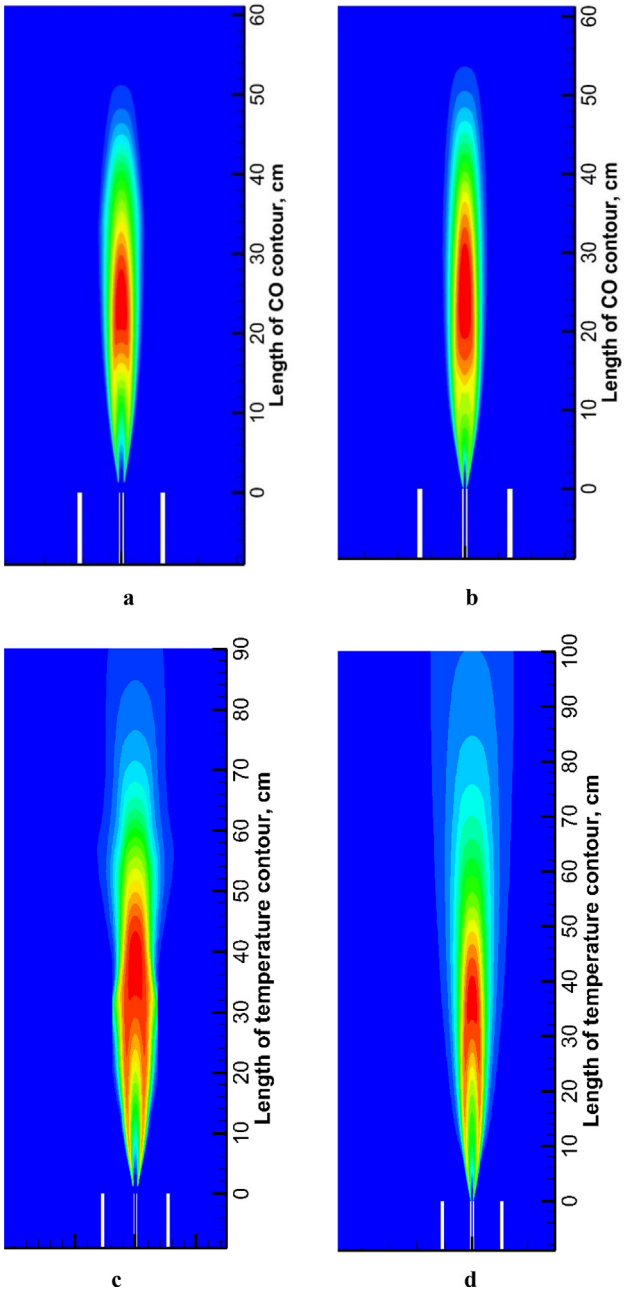

Fig. 4. Contours of carbon monoxide [a, b] and temperature [c, d] for the methane and propane flames, respectively at Re = 5700.